Environ. Water Eng., 2025, 11(1), 1-10 DOI: 10.22034/ewe.2024.441853.1914

EWE

Environment and Water Engineering

Homepage: www.jewe.ir

ISSN: 2476-3683

Synthesis of silicate nanoporous and its grafting with amine and metal ligands for the removal of Cr(VI) in industry and environment

Ghasem Zolfaghari[1]✉, and Abolfazl Zanganeh Asadabadi[1]

[1]Department of Environmental Sciences and Engineering, Faculty of Environmental Sciences, Hakim Sabzevari University, Sabzevar, Iran

ARTICLE INFO

Paper Type: Research Paper

Received: 06 February 2024
Revised: 05 May 2024
Accepted: 10 July 2024
Published: 21 March 2025

Keywords
Chromium
Grafting
Industry
Silicate nanostructure

***Corresponding author:**
G. Zolfaghari
✉ g.zolfaghari@hsu.ac.ir

ABSTRACT

The carcinogenicity and high toxicity of chromium (VI) show that the removal of this pollutant in industry, water resources, and the environment is necessary. Nanoporous materials have a high ability to remove pollutants. The aim of this study was to synthesize SBA-16 nanostructure using P123 and F127 surfactants and TEOS precursor and grafting its surface in two steps with -NH_2 (NH_2-SBA-16) and then with copper (Cu-NH_2-SBA -16). Cu-NH_2-SBA-16 was identified as a new adsorbent by XRD, SEM, EDX, and FT-IR analysis. The synthesis of nanoporous functionalized with amino group -NH_2 was done by reflux and then grafting of prepared nanoporous with copper (II) solution was performed. The maximum adsorption capacity of NH_2-SBA-16 and Cu-NH_2-SBA-16 was 6.66 and 34.48 mg/g, respectively. In addition, the kinetics of chromium adsorption followed the pseudo-second-order kinetic model. The maximum efficiency of chromium removal by Cu-NH_2-SBA-16 for contact time, initial concentration, amount of adsorbent, pH and temperature were 15 min, 10 mg/l, 1 g/l, 2, and 25 °C, respectively; adsorption capacity of Cu-NH_2-SBA-16 increased after the modification process. The synthesized nanoadsorbent with an efficiency of 90% had a spontaneous and endothermic adsorption process, and its adsorption capacity did not decrease significantly after 3 regenerations.

How to cite this paper:
Zolfaghari, G., & Zanganeh Asadabadi, A. (2025). Synthesis of silicate nanoporous and its grafting with amine and metal ligands for the removal of Cr(VI) in industry and environment. *Environ. Water Eng.*, 11(1), 12-22. doi: 10.22034/ewe.2024.441853.1914

1. Introduction

With industrial development, environmental pollution is on the rise, putting human health and the health of living organisms at risk (Esmaili Sari et al., 2007). Human activities on the path of development have had positive effects on human life, but on the other hand, they have also led to environmental pollution (Atabati et al., 2022). Potentially toxic elements are a significant group of pollutants that pose a serious threat to both the environment and human health (Zolfaghari et al., 2016; Zolfaghari et al., 2018). The ions of these potentially toxic elements have lethal and deadly effects on all forms of life and enter the food chain through waste disposal into waterways. Due to their non-biodegradability, they accumulate and their levels increase along the food chain (Zolfaghari et al., 2006). One of the most important potentially toxic elements is chromium (Cr). Its key compounds include Cr(III) chloride ($CrCl_3$), chromium nitrate, $Cr(NO_3)_3$, chromium (III) sulfate, $(Cr_3SO_4)_3$, potassium dichromate, $K_2Cr_2O_7$, and chromium (III) oxide, Cr_2O_3. These compounds are produced from various processes such as lithography, tanning, electronics, metal plating, medical devices, and the manufacture of various paints and pigments. There are reasons indicating that chromates are carcinogenic, which is why the permissible limit in drinking water is set at 0.1 mg/l (EPA, 2009). Some methods that have been used so far to remove these compounds from water sources include adsorption (Zolfaghari et al., 2011), photodegradation (Gao and Meng, 2021), sedimentation, filtration, reverse osmosis (Zolfaghari and Kargar, 2019), and ion exchange. The advantages of reverse osmosis include the removal of many water pollutants and improvement of taste and quality, while its drawbacks include high energy consumption and the need for frequent filter replacements. Ion exchange resins are widely used in separation, purification,

and disinfection processes. Their most common applications are demineralization and water treatment, but high or low temperatures can permanently risk the effectiveness of ion exchange resins. Although photodegradation is a cost-effective method, it requires the simultaneous use of catalysts to enhance efficiency.

Among the mentioned methods, adsorption technology has gained more development and application. A wide variety of adsorbents have also been used to remove these compounds. Among these adsorbents, zeolite (Kuleyin et al., 2007), activated carbon (Khaled et al., 2009), ion-exchange resins, polymeric adsorbents (Rahmanzadeh et al., 2016), carbon nanotubes, and biosorbents (Zamani et al., 2013) can be pointed out. Initially, activated carbon and zeolite were of interest due to their high adsorption capacity and availability, but the drawbacks of these adsorbents have led to a focus on a different family of adsorbents. Mesoporous materials, as a subset of nanomaterials with nano-sized pores and a very high internal surface area, have a high capability for adsorption and interaction with atoms, molecules, and ions. Mesoporous materials are generally divided into two categories based on the type of material forming the pore walls: silicate and non-silicate mesoporous materials. Among silicate mesoporous materials with structured order and narrow pore distribution, categories like M41S, SBA-n, FSM-n, and MSU-n can be mentioned. Since the 1990s, scientists have simultaneously reported silicate meso-structured materials (Kresge et al., 1992). SBA-16 has a cubic structure resembling spherical cages with *Im3m* symmetry, where each cage is connected to 8 neighboring cages through open pores. This cubic structure can sometimes also be rhombohedral or polyhedral. Modifying the surface of these mesoporous materials with organic or inorganic functional groups results in new physical and chemical properties (Zolfaghari et al., 2011). The effective removal of heavy metals from aqueous solutions has been achieved using silicate mesoporous materials functionalized with sulfonic acid, reported as a suitable and effective adsorbent for removing heavy metal ions (Qu et al. 2010). In another study, the adsorption of Pb(II), Hg(II), Cr(VI), and As(V) ions using amine-functionalized MCM-41 was investigated (Showkat et al., 2007).

So far, the modification of silica nanomaterials other than the SBA-16 version has been done using copper, but there has not been any research on the bonding of this metal agent to SBA-16. The aim of the present study was to examine the efficiency of bonded silica nanomaterials for removing chromium from water under various conditions, including contact time, initial concentration, amount of adsorbent, pH, and temperature, as well as to explore the adsorption capacity, type of adsorption, and regeneration of the adsorbent.

2. Materials and Methods

2.1 Chemicals used

The reagents utilized include tetraethyl orthosilicate (TEOS) as a silicate precursor, surfactant, hydrochloric acid (HCl), toluene, and deionized distilled water for the synthesis of mesoporous silica (SBA-16). An amine ligand was also employed to introduce amine functional groups within the structure of the mesoporous silica adsorbent. Copper was used as a metal agent for functionalizing the amine-functionalized mesoporous silica.

2.2 Synthesis of nanomaterials

2.2.1 Synthesis of silica nanoparticles

The preparation of SBA-16 silica nanoparticles involves concentrating a silica source in the presence of a template during the reaction, and eventually removing the template while linking functional groups to the silica surface. Functionalization with functional groups can be achieved in various ways as follows: i. using a modified silane, ii. simultaneous condensation of a specific silane with a silica source, and iii. grafting functional groups onto the silica. The approach of interest in the current research for synthesizing SBA-16 silica nanoparticles is the third method (Zhao et al., 1998).

2.2.2 Amine grafting to silica nanopores

The synthesis of the amine-functionalized silica nanopore adsorbent with the -NH_2 group was carried out using reflux. First, the amine ligand was added to the reflux container. Then the silica nanopore SBA-16 was added to the solution, and the resulting mixture was heated to 110 ºC. After the reflux was complete, the mixture was filtered using Whatman 41 filter paper, and the obtained residue was washed with toluene, finally leaving it to dry for 6 hours in an oven at 85 ºC. The synthesized material was named NH_2-SBA-16 (Ho et al., 2003).

2.2.3 Copper grafting to modified silica nanopores

In this step, the amine-functionalized silica nanopore with the -NH_2 group was functionalized with copper metal. To do this, the amine-functionalized silica nanopore was immersed in 100 ml of a solution containing copper (II) at room temperature. Then the modified nanopore was filtered and washed several times with distilled water. The synthesized material was named Cu-NH_2-SBA-16 (Fryxell et al., 1999).

2.3 Characteristics of the synthesized adsorbents

To identify the structure of the nanopores, X-ray diffraction (XRD) patterns of the synthesized compounds were obtained using a Philips X'Perrt MPD device within the 2theta range. To determine the shape of the prepared nanopores, a EM3200 scanning electron microscope (SEM) was used. Additionally, to specify the elemental composition of the samples, energy-dispersive X-ray spectroscopy (EDX) analysis was performed. Furthermore, the surface chemistry of the modified pores was analyzed to confirm the bonding with functional groups using Fourier-transform infrared (FT-IR-8400S) spectroscopy.

2.4 Adsorption experiments

The study of Cr(VI) adsorption from aqueous solutions was conducted in a batch system using 250 ml Erlenmeyer flasks with a solution volume of 100 ml. Initially, the main solution of chromium metal was prepared with its salt at a concentration of 500 mg/l. To investigate the factors affecting the chromium adsorption process, 0.1 g of the synthesized adsorbent (Cu-NH_2-SBA-16) was mixed with 100 ml of potassium dichromate solution using a mechanical stirrer at a speed of 150 rpm. Concentrations of 10, 17.5, 25, 32.5, and 40 mg/l were used. After that, the adsorbent was separated from the solution with the help of a vacuum pump and Whatman

filter paper, and the remaining chromium in the solution was measured using a spectrophotometer (UV-Vis Array Photonix Ar 2015) manufactured by Teifsanje Pishro Pajohesh in Iran at a maximum wavelength of 357 nm. In each experiment, the efficiency of the adsorbent was measured in two ways: the equilibrium adsorption capacity (q_e) in mg/g and the percentage of adsorption (R%). These two parameters were calculated using Equations (1) and (2):

$$q_e = (C_i - C_e)\frac{V}{m} \quad (1)$$

$$R = \frac{C_i - C_e}{C_i} \times 100 \quad (2)$$

where, C_0 and C_e are the initial and final concentrations of the compound in mg/l, V is the volume of the solution in l, and m is the mass of the adsorbent in g.

2.5 Chromium adsorption

In this study, the response surface methodology (RSM) was used to determine the testing conditions. Based on laboratory experiences, the range of experimental conditions was set for contact time between 15 to 35 minutes, initial concentration from 10 to 40 mg/l, adsorbent amount from 0.2 to 1 g/l, testing temperature from 20 to 35°C, and pH between 2 to 8. These specified ranges were input into Minitab software. Accordingly, following the central composite design of the RSM, 32 experiments were conducted in the lab under the above conditions. To find the optimal concentration of this variable, adsorption was examined at concentrations of 10, 17.5, 25, 32.5, and 40 mg/l. In these processes, the pH of the solution for chromium was considered to be 6, and the amount of adsorbent used in these experiments was set at 1 g/l. To evaluate the effect of adsorbent quantity on adsorption capacity, different amounts of the Cu-NH_2-SBA-16 adsorbent (0.2, 0.4, 0.6, 0.8, and 1 g/l) were added to 100 ml of 10 ppm chromium solutions. Each of these solutions was stirred for 15 minutes with a mechanical stirrer. The solutions were then filtered, and the chromium concentration in the filtrate was measured using a UV-Vis spectrophotometer. Changing the pH is one of the important parameters in optimizing the adsorption process. To investigate the effect of pH on the adsorption process, the pH of the metal solution was adjusted to values of 2, 3.5, 5, 6.5, and 8 (considering the KSP (solubility product constant) related to each metal at the desired concentration) using 1N hydrochloric acid and sodium hydroxide (pH meter: Eutech300, Singapore). These tests were carried out with an adsorbent dose of 0.1 g/l and a metal concentration of 100 mg/l. In this study, to assess the effect of temperature on the adsorption rate, temperatures of 20, 23.75, 27.5, 31, and 35°C were investigated. Contact times of 15, 20, 25, 30, and 35 minutes were examined to analyze the effect of contact time of the adsorbent with the pollutant solution (the investigation of contact time at the mentioned times was after it was identified in previous experiments that lower times than one hour had greater adsorption efficiency).

2.6 Kinetics, regeneration, and thermodynamic

Among the most commonly used kinetic models are the pseudo-first-order kinetic model and the pseudo-second-order kinetic model. To calculate the adsorption capacity qt in terms of (mg/g), Eq. (3) was used:

$$q_t = (C_o - C_t)\frac{V}{W} \quad (3)$$

where, q_t is the adsorption capacity at time t in (mg/g), and C_t is the concentration of the pollutant compound in the solution at time t in (mg/l). W is the mass of the adsorbent in g.

In this study, the regeneration of the synthesized nanoadsorbent was carried out using 0.1 molar nitric acid. The nanoadsorbent was stirred with nitric acid for 2 hours at room temperature. Then, the mixture of adsorbent and acid was filtered using filter paper, washed with water, and dried in an oven. With the amount of chromium released in the aqueous solution (C_{des}) and the amount of chromium adsorbed on the nanoadsorbent (C_{ads}), the chromium recovery efficiency can be calculated as Eq. (4):

$$R(\%) = \frac{C_{des}}{C_{ads}} \times 100 \quad (4)$$

The regenerated nanoadsorbent was again used to remove chromium at a temperature of 20 °C, with a pH of 6, an adsorbent amount of 0.8 g/l, and a time of 35 minutes. This experiment was repeated three times. The results showed that there was no significant decrease in the adsorption capacity of the nanoparticles.

The thermodynamic variables of adsorption at a concentration of 20 mg/l, pH=6, adsorbent amount of 0.8 g, and for 35 minutes at temperatures of 293, 303, and 313 Kelvin were calculated. Thermodynamic variables such as Gibbs free energy, changes in enthalpy (ΔH), and changes in entropy can be investigated and calculated using the changes in equilibrium constants with temperature in equilibrium conditions. The change in Gibbs free energy for the adsorption reaction was calculated using Eq. (5):

$$\Delta G° = -RTLnK_d \quad (5)$$

where, $\Delta G°$ is the standard free energy change in joules, R is the universal gas constant with a value of 8.314 J/K.mol, and T is the absolute temperature in Kelvin. The equilibrium constant was calculated using Eq. (6) (Manirethan et al., 2018):

$$K_d = \frac{AV}{SM} \quad (6)$$

where, A is the amount of heavy metal adsorbed by the adsorbent, V is the volume of the solution in ml, S is the amount of heavy metal remaining in the solution, and M is the mass of the adsorbent in grams. On the other hand, by plotting a linear graph of the standard free energy change with temperature using Eq. (7), we can calculate the standard entropy change of adsorption ($\Delta S°$) and the standard enthalpy change of adsorption (Manirethan et al., 2018):

$$\Delta G° = \Delta H° - T\Delta S° \quad (7)$$

3. Results and Discussion

3.1 Identification and specification of the adsorbents

3.1.1 Examination of X-ray diffraction spectra

Fig. 1 displays the XRD spectra of the functionalized and non-functionalized silica nanomaterials. The X-ray diffraction pattern of these nanomaterials can reveal insights into their pore structures. The XRD spectrum for the silica nanomaterial shows a prominent peak corresponding to the crystalline plane (110) at an angle of 2θ, indicating a regular structure for the silica nanomaterial. Additionally, another peak corresponding to the crystalline plane (200) is observed at an angle of 2θ,

which is characteristic of SBA-16. By functionalizing the surface of the silica nanomaterial, the regular pore structure is maintained, and only a decrease in the peak intensity for the functionalized silica nanomaterial is noted, proving that the structure of the silica nanomaterial remains intact after functionalization. In other words, the intensity of the peaks related to NH_2-SBA-16 is nearly equal to the intensity of the peaks of SBA-16, and these peaks have remained well defined, indicating that the NH_2-SBA-16 synthesized through the grafting method retains a highly ordered hexagonal structure similar to that of SBA-16. The XRD diffraction pattern aligns with that from previous studies (Zhao et al., 1998).

3.1.2 Scanning electron microscope image

Scanning electron microscope (SEM) images of the silicate nanopore composition are shown in Fig. 2(a). As can be seen, the morphology of the particles shown is mostly spherical, which is consistent with the *Im3m* crystal model. The granular structure of the sample is preserved. It is observed that the spherical morphology and structure of SBA-16 is preserved after functionalization with the amino -NH_2 group, and the functional groups located on the surface of SBA-16 are clearly visible (Fig. 2b). The spherical and multifaceted structure of the silicate nanopore is also visible (Fig. 2c). Moreover, the preservation of the initial morphology after functionalization with the metal ligand is evidence of the correctness of the process.

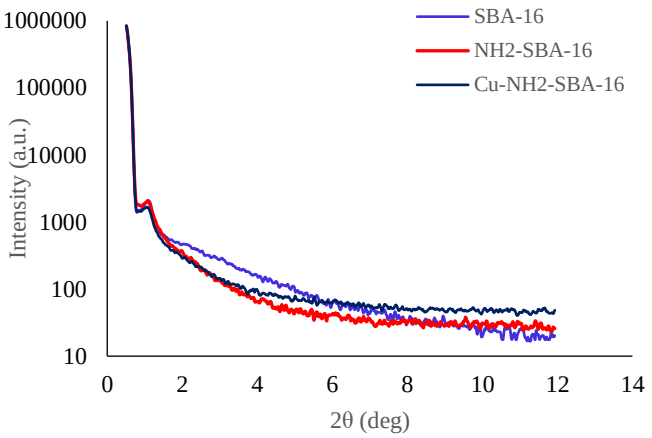

Fig. 1 XRD pattern of SBA-16, NH_2-SBA-16, and Cu-NH_2-SBA-16

3.1.3 EDX analysis

Energy dispersive X-ray spectroscopy (EDS or EDX) is an analytical method used to analyze the structure, or chemical properties, of a sample (Najafian et al. 2015). The EDX spectrum is a graph drawn based on the X-ray energy received from each energy level. Each peak shown in this graph is specific to an atom and therefore represents an element.

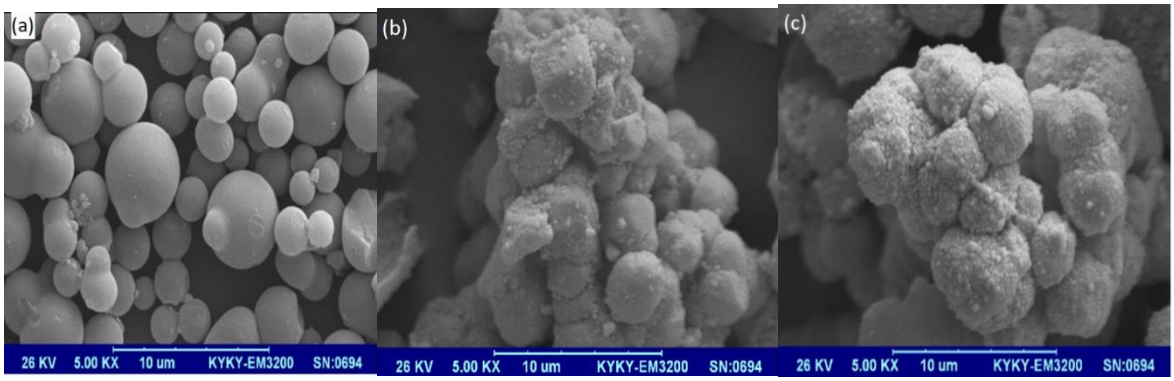

Fig. **2** SEM images of synthesized samples. a**)** SBA-16, b) SBA-16, NH_2-SBA-16, and c) SEM image of Cu-NH_2-SBA-16

Peaks with higher heights in the spectrum mean a higher concentration of the element in question in the sample. The results of the EDX spectrum analysis of the SBA-16, NH_2-SBA-16, and Cu- NH_2- SBA-16 samples are shown in Table 1. As the aforementioned table shows, the presence of nitrogen and carbon elements in the NH_2- SBA-16 sample indicates the occurrence of the correct bonding process of the amino group NH_2. Similarly, Table 1 shows that the element copper in the sample Cu-NH_2-SBA-16 has been added to the analysis composition, indicating the correct bonding of the copper metal agent.

Table 1 Elemental analysis of SBA-16, NH_2-SBA-16, and Cu-NH_2-SBA-16

Adsorbents	Elements	Atomic percentage	Normal percentage
SBA-16	Oxygen	64.30	50.65
	Silica	35.70	49.35
NH_2-SBA-16	Oxygen	53.81	45.69
	Nitrogen	8.52	6.33
	Silica	28.10	41.89
	Carbon	9.57	6.10
Cu- NH_2-SBA-16	Oxygen	59.32	49
	Nitrogen	8.21	5.94
	Silica	25.55	37.04
	Copper	1.41	4.61
	Carbon	5.51	3.42

3.1.4 FT-IR Spectroscopy

This method was used with the aim of qualitatively identifying the silicate adsorbent SBA-16 and the amine group NH_2. For this purpose, the FTIR spectrum was performed in the wavenumber range of 400-4000 cm^{-1}. In the spectrum related to SBA-16, a broad peak is seen in the range of 811-1068 cm^{-1}, which is characteristic of Si-O-Si. The peak found in the

range of 811-1068 cm^{-1} also indicates the presence of the -OH group in the adsorbent. It's worth noting that the surfactant creates a peak in the range of 2300-2400 cm^{-1}, and the absence of this peak indicates that the surfactant removal process has been carried out effectively. In the spectrum related to the amine-functionalized adsorbent with -NH_2, the peak present in the range of 1570 cm^{-1} indicates the presence of the -NH_2 amine group on the silicate adsorbent. Another peak is observed in the wavelength range of 2854-2958, which corresponds to the propylamine (C-H) group (Anbia and Lashgari, 2009). These results indicate that the functionalization process was successful and confirm the presence of the mentioned functional groups on the surface of the nanocavity. The analysis of the data obtained from the spectroscopy related to SBA-16 and NH_2- SBA-16 adsorbents is presented in Fig. 3.

3.2 Study of the adsorption process

3.2.1 Impact of initial chromium concentration

The effect of the initial concentration of the solution on the amount of Cr adsorption at different concentrations of 10, 17.5, 25, 32.5, and 40 mg/l was studied, and the results of these studies are shown in Fig. 4. As seen in Fig. 4(a), with the increase of the initial concentration of the solution from 10 mg/l to 40 mg/l, the amount of adsorption decreases from 92% to 45%, indicating that at higher concentrations, the rate of increase in adsorption due to the rise in initial concentration is less. These observations can be explained by the fact that at initial concentrations, species have better access to the active sites of the adsorbent, and the active sites available for further adsorption will not have an increasing trend (Wan Ngah and Hanafiah, 2008).

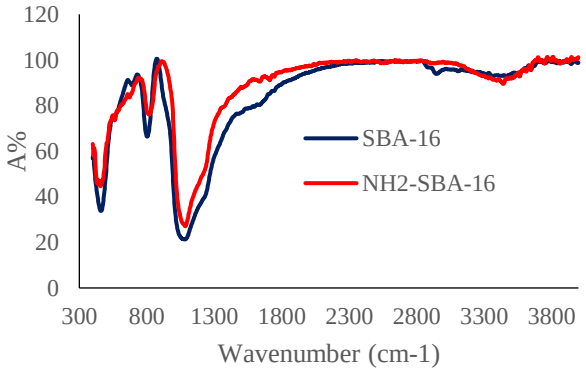

Fig. 3 FT-IR spectra of synthesized samples (SBA-16, and NH_2-SBA-16)

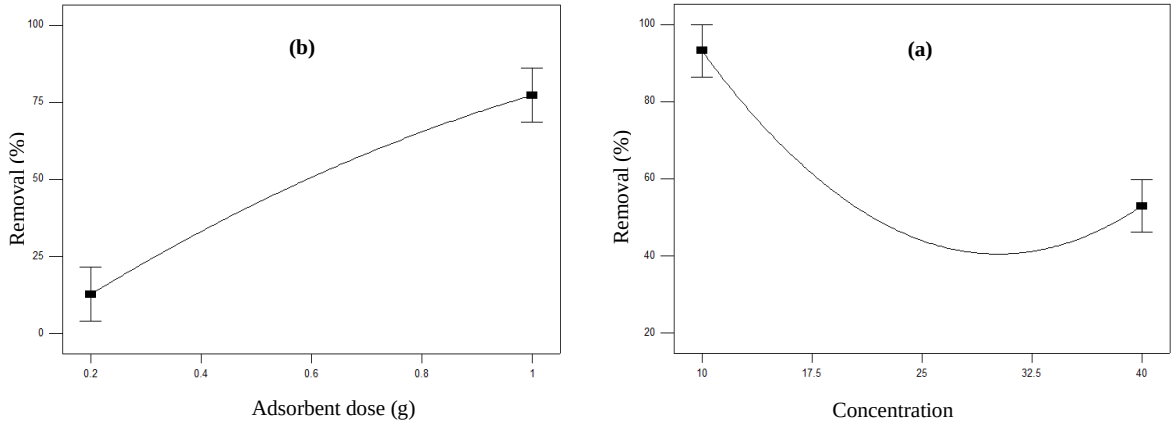

Fig. 4 Effect of different conditions on chromium removal rate onto Cu-NH_2-SBA-16: a) The effect of concentration (time: 15 min, dose: 0.8 g, pH: 6, and temperature: 25 C˚) and b) Dose (time: 15 min, concentration: 20 mg/l, pH: 6, and temperature: 25 °C)

3.2.2 Effect of adsorbent amount

Fig. 4(b) shows that the adsorption percentage increases significantly with increasing adsorbent amount. By increasing the adsorbent amount from 0.2 to 1 g/l, the adsorption percentage increases rapidly to 76%. This is due to the increase in the active sites of the adsorbent. The results obtained in various studies show that with increasing the adsorbent amount, the adsorption percentage increases linearly, but the efficiency of the adsorbent, which is usually calculated with the parameter (q_e), does not change linearly, but rather reaches its optimum value at a certain adsorbent amount, which must be calculated for each adsorbent. In one study, aminopropyl-functionalized MCM-41 was used to remove potentially toxic elements (Benhamou et al., 2009).

3.2.3 Effect of pH

The pH of the solution can affect the adsorbent surface by protonating the functional groups. If the potentially toxic element of interest is a metal cation, it has usually been shown that it shows better adsorption at intermediate or high pH, because at low pH the H^+ ions in the solution increase and compete with the metal cations. While the opposite is true for elements that are in the form of anions, such as Cr(VI) and As(V) (Showkat et al., 2007). At high pH, the divalent ions $CrO_4^{2-}/Cr_2O_7^{2-}$ increase. Basically, hexavalent chromium exists in the form of chromic acid at very acidic pHs and is immediately converted to acidic hydrogen chromate $HCrO^{4-}$ at different concentrations and up to a pH of 6.5. Since chromium divalent ions have a negative charge, there is competition between these ions and OH^- ions at high pH, so the adsorption rate is higher in acidic environments. In another study, the adsorption of Remazol on HMS nanopores was investigated (Asouhidou et al., 2009). The results of this study indicate that the adsorption rate increases significantly with decreasing pH. The effect of pH on the adsorption rate is shown in Fig. 5(a). In this study, the point zero pH (pH_{zpc}) was determined to be

4.9. The surface of the silicate nanoparticle is negative at pH levels above pH_{zpc}, creating an electrostatic repulsion between the negatively charged silicate nanoparticle and the negatively charged bivalent chromium ions. Additionally, at pH levels lower than 9.4, the surface of the silicate nanoparticle is positive, resulting in a strong electrostatic attraction between the surface groups and the negatively charged bivalent chromium ions.

3.2.4 Effect of temperature

Another influential factor in the Cr adsorption process is temperature. The results of this project indicated that the adsorption rate was higher at mid-range temperatures compared to minimal and maximal states. The effect of temperature on the adsorption rate is illustrated in Fig. 5(b). The penetration of Cr into the Cu-NH_2-SBA-16 nanoadsorbent increased somewhat with rising temperatures. This suggests that a greater chemical interaction occurs between the adsorbate and the surface functional groups of Cu-NH_2-SBA-16. As previously reported, the efficiency of adsorption tends to increase somewhat with higher temperatures. Some studies indicate that raising the temperature results in a higher removal efficiency of metals on activated carbon (Seco et al., 1997).

3.2.5 Effect of contact time

As seen in Fig. 5(c), the contact time within the specified range has a lesser effect on the Cr adsorption level compared to other evaluated factors. Nevertheless, the adsorption rate begins to decline slightly after reaching equilibrium (15 min); in other words, as the contact time exceeds the equilibrium period, the adsorption rate not only fails to increase but starts to decrease. Time is a determining factor in the adsorption process, and it appears that as the contact time of the adsorbent with the adsorbed ions increases, the amount of adsorption increases. Most studies have shown that the highest adsorption usually occurs within the first few minutes. This may relate to the fact that initially, there are many vacant sites available for ion adsorption, and the concentration gradient of ions to the adsorbent is very high (Guerra, 2010).

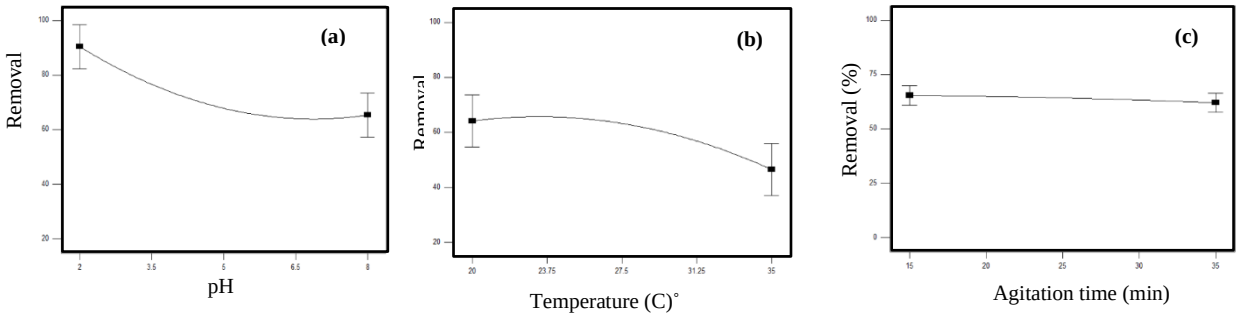

Fig. 5 Effect of different conditions on chromium removal rate onto Cu-NH_2-SBA-16: a) pH (time: 15 min, concentration: 20 mg/l, dose: 0.8 g, and temperature: 25 C˚), b) temperature (time: 15 min, concentration: 20 mg/l, dose: 0.8 g/l, and pH: 6) and c) time (concentration: 20 mg/l, dose: 0.8 g, temperature: 25 C˚, and pH: 6).

3.3 Adsorption isotherms

There are various isotherms to study and design adsorption systems, such as the Langmuir, Freundlich, Bohart-Adams, Brunauer-Emmett-Teller, Dubinin-Radushkevich, Florry-Huggins, Frenkel-Halsey-Hill, Redlich-Peterson, Temkin, Elovich, and Langmuir isotherms, among others (Benjelloun et al. 2021). The Langmuir equation, which determines the amount of material adsorbed and its concentration in the solution, is expressed as Eq. (8) (Benhamou et al., 2009):

$$C_e/q_e = 1/q_m b + (1/q_m)\, C_e \quad (8)$$

Where, q_e (mg/g) is the amount adsorbed at equilibrium concentration C_e (mg/l), q_m (mg/g) is the Langmuir constant representing the maximum monolayer capacity, and b is the Langmuir constant associated with the energy of adsorption. The Freundlich isotherm also provides an empirical method that describes a scenario where the species is adsorbed in a heterogeneous manner on the surface. The Freundlich relation explains heterogeneous adsorption and is expressed as Eq. (9) (Benhamou et al., 2009):

$$ln\ q_e = ln\ K_f + (1/n)\ ln\ C_e \quad (9)$$

Where, C_e (mg/l) is the equilibrium concentration of the metal ion, q_e (mg/g) is the amount adsorbed, K_f is a constant related to adsorption capacity, and n is an empirical constant related to the intensity of adsorption. Various studies have utilized both linear and nonlinear models of adsorption isotherms. In this study, the linear models of the Langmuir and Freundlich isotherms have been used. According to the R^2 value, which indicates the linearity and correlation of the curve obtained from drawing the adsorption isotherm diagrams, the adsorption mechanism of chromium on the adsorbent Cu-NH_2-SBA-16 aligns more with the Freundlich isotherm, while on the adsorbent NH_2-SBA-16, it aligns with the Langmuir isotherm (Table 2). The R^2 value closer to one indicates higher conformity with that isotherm; thus, it can be said that chromium is adsorbed in a heterogeneous manner on the adsorbent Cu-NH_2-SBA-16 and in a homogeneous manner on the adsorbent NH_2-SBA-16.

As shown in Table 2, the isotherm constants of Langmuir and Freundlich (q_m and K_f) for the metal-functionalized adsorbent indicate a higher number. In other words, the maximum adsorption in the Cu-NH_2-SBA-16 adsorbent is significantly greater than that in the NH_2-SBA-16 adsorbent. Therefore, other adsorption studies will be conducted using the Cu-NH_2-SBA-16 adsorbent. The Freundlich constant, K_f, which indicates the adsorption capacity of the adsorbent, was determined to be 1.34 and mg/g 8.014 for NH_2-SBA-16 and Cu-NH_2-SBA-16, respectively. These values show a similar trend to the Langmuir constant, qm. The constant n represents

the relative magnitude and diversity of the energies associated with the adsorption of lead onto the adsorbents. The values of in are greater than one (1.9 and 3.1), indicating a high intensity of adsorption (Benhamou et al., 2009).

Table 2 Freundlich and Langmuir parameters for adsorption of Cr(VI) onto Cu-NH_2-SBA-16.

Adsorbent	Freundlich			Langmuir		
	R^2	n (l/mg)	K_f (mg/g)	R^2	b (l/mg)	q_m (mg/g)
Cu-NH_2-SBA-16	0.997	3.1	8.014	0.988	1.07	34.48
NH_2-SBA-16	0.936	1.9	1.34	0.953	0.237	6.66

In other words, the tendency and intensity of adsorption increase in the order of NH_2-SBA-16 < Cu-NH_2-SBA-16. Copper (II) ions are attached to ethylene diamine (EDA) ligands to form octahedral complexes on the surface of mesoporous silica. This creates hosts with positive charges exhibiting multiple symmetries that correspond to the geometry of tetrahedral anions. The attachment of pollutant anions occurs through an electrostatic coordination force with the Cu (II) center. In a study, a biosorbent (the bark of the Platanus orientalis tree) was investigated for the removal of nickel and chromium (VI) from electroplating wastewater as a real sample (Akar et al., 2019). According to the mentioned study, *P. orientalis* can be a cost-effective and efficient biosorbent for the adsorption and removal of chromium (VI) and nickel from electroplating wastewater. However, it appears that this adsorbent is more effective for chromium (VI) with a moderate removal efficiency of 90.15% compared to nickel, with an average removal efficiency of 65.75%.

3.4 Reaction kinetics

3.4.1 Pseudo-first-order model

Various studies have utilized linear and nonlinear kinetic adsorption models. In this research, a linear kinetic reaction model has been employed (Ho et al., 2003). The simplest kinetic model is the pseudo-first-order model. This model was proposed by Lagergren and is expressed in the form of Eq. (10) (Hamadi et al., 2002):

$$ln\ (q_e - q_t) = lnq_e - K_1 t \qquad (10)$$

q_t and q_e represent the equilibrium adsorption capacity of the species of interest at time t and at equilibrium, measured in mg/g. k_1 is the rate constant of the pseudo-first-order Equation. The curve of $ln\ (q_e - q_t)$ versus t for chromium is shown in Fig. 6. The results obtained from these graphs are also mentioned in Table 3. As the table shows, the obtained adsorption capacity values are quite different from what the model predicts. The correction coefficients are also small. Therefore, the adsorption process on the adsorbent does not follow a pseudo-first-order kinetic model.

3.4.2 Pseudo-second-order kinetic model

If the adsorption rate has a second-order mechanism, the second-order kinetic rate Equation is expressed by McKay as Equation (11) (Hamadi et al., 2002):

$$t/q_t = 1/K_2 q_e^2 + (1/q_e)\ t \qquad (11)$$

In the above Equation, K_2 is the equilibrium rate constant (g/mg min). If the kinetic model of the adsorption process follows the pseudo-second-order model, the curve of t/q_t versus t will be a straight line from which the rate constants can be derived. These curves for chromium are shown in Fig. 6, and the rate constants as well as the correction factors are presented in Table 3 respectively. It is observed that the obtained values align with the observed values, and it is anticipated that the adsorption kinetic pattern for the adsorbent follows the pseudo-second-order kinetic model.

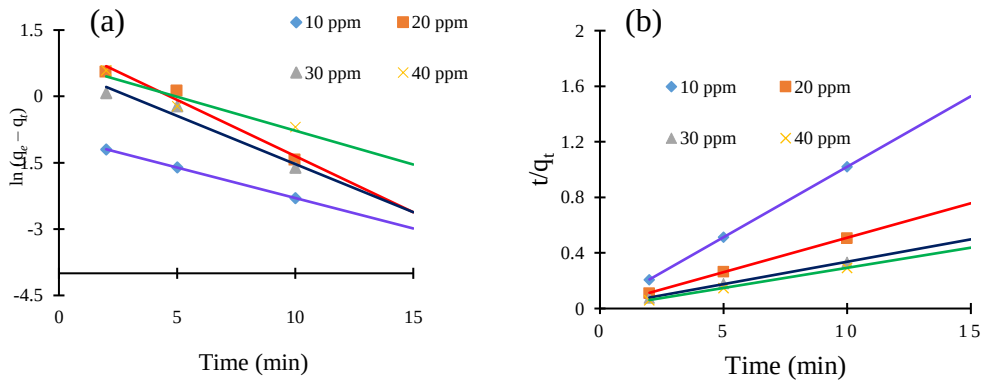

Fig. 6 Linearization of Cr adsorption kinetic onto Cu-NH_2-SBA-16: a) Pseudo-first order rate and b) Pseudo-second order rate

Based on the values of the correction factors, the best kinetic model that describes this type of adsorption is the pseudo-second-order model. The calculated adsorption capacity values derived from this model are also closer to the experimental values. Furthermore, as the initial concentration of the solution increases, the linearity of the resulting curve becomes more apparent. When the initial concentration of chromium increases from 10 to 40 mg/l, the value of K decreases from 1.67 to 0.50 g/mg.min for Cu-NH_2-SBA-16. This means that K is dependent on C_0. The rate of adsorption decreases with increasing initial concentration. The results in Table 3 confirm this claim. Similar results have also been obtained in other studies (Hamadi et al., 2002). The results of the linear kinetic models indicate that the linear curves have a

high capability in predicting the adsorption kinetic pattern since it is observed that the values obtained from the model are consistent with the observed experimental values.

Table 3 Kinetic adsorption parameters obtained using pseudo-first-order and pseudo-second-order models for the removal of Cr by Cu-NH_2-SBA-16

Concentration	Pseudo-first-order			Pseudo-second-order			Exprimental q_e (mg/g)
	Computational q_e (mg/g)	K_1 (l/min)	R^2	Computational q_e (mg/g)	K_2 (g/mg.min)	R^2	
10	2.508	0.011	0.999	9.98	1.67	0.999	9.9
20	3.292	0.009	0.969	20.4	1.60	0.999	19.94
30	1.914	0.007	0.955	31.25	0.60	0.999	28.60
40	2.135	0.006	0.915	34.48	0.50	0.999	34.60

3.5 Thermodynamic variables and regeneration of nanoadsorbents

The value of equilibrium constant, K_d for chromium adsorption on the Cu-NH_2-SBA-16 adsorbent was calculated to be 1500, 1250, and 1022 as the temperature increased. Similarly, the value of $\Delta G°$ for the aforementioned data was obtained as -17870, -18019, and -18088 J/mol. According to Equation (7), by plotting a linear graph of the Gibbs free energy change of the adsorption process with temperature, the entropy change (10.9 J/K·mol) was calculated from the slope of the line, and the enthalpy change (14690 J/mol) was derived from the y-intercept. It can be observed that as temperature increases, the standard Gibbs free energy decreases. On the other hand, changes in the standard Gibbs free energy at different temperatures indicate a linear behavior with a good correlation coefficient between these two factors (R^2=0.95). The results showed that the standard enthalpy change is -14690 J/mol and the standard entropy change is 9.10 J/K·mol. The negative value of the standard Gibbs free energy for the system indicates that the adsorption process occurs spontaneously. Additionally, the positive value of the standard enthalpy change for the adsorption reaction suggests that the process is endothermic. The positive value of the standard entropy change for the system also indicates an increase in disorder at the interface of the solid/solution adsorption process. The results of the regeneration of the nanoadsorbent showed that there was no significant decrease in the capacity to absorb nanoparticles.

4. Conclusion

According to the results of this study, the following can be concluded:

1. In this research, the effective and fast removal of chromium was done by copper(II) functionalized silicate nanoporous (Cu-NH_2-SBA-16). Experiments show that in a short time of 15 minutes, the adsorption capacity reaches its maximum value, which indicates the high speed of adsorption on the adsorbent.

2. Increasing the amount of absorbent increases the surface area of the adsorbent, which leads to an increase in the contact surface of the adsorbent with the adsorbed species, and the percentage of adsorption increases.

3. From all the studies, it can be concluded that the power of the adsorbent functionalized with copper(II) ions has increased significantly in removing chromium.

4. The chemical structure of the adsorbent consists of silicate sources and ammonium and copper ligands, all of which are compatible with the environment. The removal efficiency of 90% of the synthesized adsorbent shows that this adsorbent is an effective material for chromium removal.

The need for multiple equipment to identify nanoadsorbents and their unavailability is one of the limitations of such research. In the end, it is suggested to use the modified nanopore in this study to check the efficiency of removing other toxic elements such as cadmium, lead, arsenic, and mercury. Also, the use of other optimization methods such as Taguchi using the mentioned nanoadsorbent will be very attractive. It is necessary to investigate the economic aspects of using the adsorbent in future studies.

Acknowledgement

The Iran Nanotechnology Innovation Council is acknowledged for its participation. Thanks are also extended to the Vice Presidency for Science and Technology and the National Elites Foundation.

Data Availability

The data used in this research are presented in the text of the article.

Conflicts of interest

The authors of this paper declared no conflict of interest regarding the authorship or publication of this paper.

Author contribution

G. Zolfaghari: Modeling and Results Analysis; A. Zanganeh Asadabadi: Results Analysis and Research Management; Research Management; Data Collection.

References

Akar, S., Lorestani, B., Sobhanardakani, S., Cheraghi, M., & Moradi, M. (2019). Surveying the efficiency of *Platanus orientalis* bark as biosorbent for Ni and Cr(VI) removal from plating wastewater as a real sample. *Environ. Monit. Assess. 191*(6), 373. https://doi.org/10.1007/s10661-019-7479-z.

Anbia, M., & Lashgari, M. (2009). Synthesis of amino-modified ordered mesoporous silica as a new nano sorbent for the removal of chlorophenols from aqueous media. *J. Chem. Eng. 150* (2-3), 555-560. https://doi.org/10.1016/j.cej.2009.02.023.

Atabati, A., Adab, H., Zolfaghari, G., & Nasrabadi, M. (2022). Modeling groundwater nitrate concentrations using spatial and non-spatial regression models in a semi-arid environment. *Water Sci. Eng. 15* (3), 218-227. https://doi.org/10.1016/j.wse.2022.05.002.

Asouhidou, D. D., Triantafyllidis, K. S., Lazaridis, N. K., & Matis, K. M. (2009). Adsorption of Remazol Red 3BS from aqueous solutions using APTES- and cyclodextrin-modified HMS-type mesoporous silicas. *Colloid. Surf. 346*(1-3), 83-90. https://doi.org/10.1016/j.colsurfa.2009.05.029.

Benhamou, A., Baudu, M., Derriche, Z., & Basly, J. P. (2009). Aqueous heavy metals removal on amine-functionalized Si-MCM-41 and Si-MCM-48. *J. Hazard. Mater. 171(1-3)*, 1001-1008. https://doi.org/10.1016/j.jhazmat.2009.06.106.

Benjelloun, M., Miyah, Y., Evrendilek, G. A., Zerrouq, F., & Lairini, S. (2021). Recent advances in adsorption kinetic models: their application to dye types, *Arab. J. Chem. 14*(4), 103031. https://doi.org/10.1016/j.arabjc.2021.103031.

Esmaili Sari, A., Zolfaghari, G., Ghasempouri, S. M., Shayegh, S. S, & Hasani Tabatabei, M. (2007). Effect of age, gender, years of practice, specialty and number of amalgam restorations on mercury concentration in nails of dentists practicing in Tehran. *J. Iran. Dent. Assoc., 19*(1), 97-104 [in Persian].

EPA (2009). National Primary Drinking Water Regulation Table. https://www.epa.gov/ground-water-and-drinking-water/national-primary-drinking-water-regulation-table.

Fryxell, G. E., Liu, J., Hauser, T. A., Nie, Z., Ferris, K. F., Mattigod, S., Gong, M., & Hallen, R. T. (1999). Design and synthesis of selective mesoporous anion traps. *Chem. Mater. 11*(8), 2148-2154. https://doi.org/10.1021/cm990104c.

Gao, X., & Meng, X. (2021). Photocatalysis for heavy metal treatment: A review. *Process., 9*, 1729. https://doi.org/10.3390/pr9101729.

Guerra, D. L., Oliveira, H. C. P., Correa da Costa, P. C., Viana, R. R., & Airoldic, C. (2010). Adsorption of chromium(VI) ions on Brazilian smectite: Effect of contact time, pH, concentration, and calorimetric investigation. *CATENA, 82*(1), 35-44. https://doi.org/10.1016/j.catena.2010.04.008.

Hamadi, N. K., Chen, X. D., Farid, M. M., & Lu, M. G. Q. (2001). Adsorption kinetics for the removal of chromium(VI) from aqueous solution by adsorbents derived from used tyres and sawdust. *Chem. Eng. J., 84*, 95-105. https://doi.org/10.1016/S1385-8947(01)00194-2

Ho, K. Y., McKay, G., & Yeung, K. L., (2003). Selective adsorption from ordered mesoporous silica. *Langmuir. 19*, 3019-3024. https://doi.org/10.1016/S0167-2991(04)80581-0.

Khaled, A., El Nemr, A., El-Sikaily, A., & Abdelwahab, O. (2009). Removal of direct N Blue-106 from artificial textile dye effluent using activated carbon from orange peel: Adsorption isotherm and kinetic studies. *J. Hazard. Mater. 165*, 100–110. https://doi.org/10.1016/j.jhazmat.2008.09.122.

Kresge, M. E., Leonowicz, W. J., Roth, J. C., Vartuli, J. C., & Beck, J. S. (1992). Ordered mesoporous molecular sieves synthesized by a liquid-crystal template mechanism. *Nat. 359(6397)*, 710-712. https://doi.org/10.1038/359710a0.

Kuleyin, C. (2007). Removal of phenol and 4-chlorophenol by surfactant-modified natural zeolite. *J. Hazard. Mater.144*, 307–315. https://doi.org/10.1016/j.jhazmat.2006.10.036.

Manirethan, V., Raval, K., Rajan, R., Thaira, H., & Balakrishnan, R. M. (2018). Kinetic and thermodynamic studies on the adsorption of heavy metals from aqueous solution by melanin nanopigment obtained from marine source: *Pseudomonas stutzeri*. *J. Environ. Manag. 214*, 315-324. https://doi.org/10.1016/j.jenvman.2018.02.084

Najafian, A., Rabbani, M., Rahimi, R., Deilamkamar, M., & Maleki, A. (2015). Synthesis and characterization of copper porphyrin into SBA-16 through "ship in a bottle" method: a catalyst for photo oxidation reaction under visible light. *Solid State Sci. 46*, 7-13. https://doi.org/10.1016/j.solidstatesciences.2015.05.005.

Qu, Q., Gu, Q., Gu, Z., Shen, Y., Wang, C., & Hu, X. (2012). Efficient removal of heavy metal from aqueous solution by sulfonic acid functionalized nonporous silica microspheres. *Colloid. Surf. A Physicochem. Eng. Asp. 415*, 41–46. https://doi.org/10.1016/j.colsurfa.2012.08.059.

Rahmanzadeh, L., Ghorbani, M., & Jahanshahi, M. (2016). Effctive removal of hexavalent mercury from aqueous solution by modifid polymeric nanoadsorbent. *J. Water Environ. Nanotechnol. 1*, 1-8. https://doi.org/10.7508/jwent.2016.01.001.

Showkat, A. M., Zhang, Y. P., Kim, M. S., Gopalan, A. I., Reddy, K. R., & Lee, K. P. (2007). Analysis of heavy metal toxic ions by adsorption onto amino-functionalized ordered mesoporous silica. *Bull. Korean. Chem. Soc. 28*, 1985–1992. https://doi.org/10.5012/bkcs.2007.28.11.1985.

Seco, A., Marzal, P., & Gabaldo, C. (1997). Adsorption of heavy metals from aqueous solutions onto activated carbon in single Cu and Ni systems and in binary Cu.Ni, Cu.Cd and Cu.Z systems. *J. Chem. Technol. Biotechnol. 68,* 23-30. https://doi.org/10.1016/j.jhazmat.2023.131106.

Wan Ngah, W. S., & Hanafiah, M. A. (2008). Removal of heavy metal ions from wastewater by chemically modified plant wastes as adsorbents a review. *Bioresour. Technol. 99(10),* 3935. https://doi.org/10.1016/j.biortech.2007.06.011.

Zamani, A. A., Shokri, R., Yaftian, M. R., & Parizanganeh, A. H. (2013). Adsorption of lead, zinc and cadmium ions from contaminated water onto Peganum harmala seeds as biosorbent. *Int. J. Environ. Sci. Technol*. *10,* 93-102. https://doi.org/10.1007/s13762-012-0107-x

Zhao, D., Huo, Q., Bradley, J. F., Chmelka, F., & Galen, D. (1998). Nonionic triblock and star diblock copolymer and oligomeric surfactant symtheses of highly ordered, hydrothermally stable, mesoporous silica structures. *J. Am. Chem. Soc. 120,* 6024-6036. https://doi.org/10.1021/ja974025i.

Zolfaghari, G. (2018). Risk assessment of mercury and lead in fish species from Iranian international wetlands. *MethodsX*, *5*, 438–447. https://doi.org/10.1016/j.mex.2018.05.002

Zolfaghari, G., & Kargar, M. (2019). Nanofiltration and microfiltration for the removal of chromium, total dissolved solids, and sulfate from water. *MethodsX*, *6*, 549–557. https://doi.org/10.1016/j.mex.2019.03.012

Zolfaghari, G., Delsooz, M., & Rajaee, S. (2016). Study of mercury pollution in water, sediments, and fish from Hamoon international wetland. *J.Water Wastewater, 27(5),* 25-37 [in Persian].

Zolfaghari, G., Esmaili Sari, A., Ghasempouri, S. M., Ghorbani, F., Ahmadifard, N., & Shokri, N. (2006). Relationship beetween age, gender and weight with mercury concentration in different organs of *Chalcalburnus chalcalburnus* from Anzali wetland. *Iran. J. Mar. Sci. Technol. 5*(3-4), 23-31 [in Persian].

Zolfaghari, G., Esmaili-Sari, A., Unesi, H., & Anbia, M. (2011). Surface modification of ordered nanoporous carbons CMK-3 via a chemical oxidation approach and its application in removal of lead pollution from water. *Int. Proc. Chem. Biol. Environ. Eng.* 2174–2178.